Pergamon
www.elsevier.com/locate/asr

Adv. Space Res. Vol. 27, No. 11, pp. 1831–1836, 2001

Printed in Great Britain
0273-1177/01 $20.00 + 0.00
PII: S0273-1177(01)00333-7

MAGNETIC FIELD DRAPING AROUND MARS: MARS GLOBAL SURVEYOR RESULTS

D. Crider[1], M. Acuña[1], J. Connerney[1], D. Mitchell[2], R. Lin[2], P. Cloutier[3], H. Rème[4], C. Mazelle[4], D. Brain[5], N. Ness[6], and S. Bauer[7]

[1] *NASA Goddard Space Flight Center, Greenbelt, MD, USA*
[2] *Space Science Laboratory, U. California, Berkeley, CA , USA*
[3] *Physics and Astronomy, Rice U., Houston, TX , USA*
[4] *Centre d'Etude Spatiale des Rayonnements, Toulouse, France*
[5] *U. Colorado, Boulder, CO, USA*
[6] *Bartol Research Institute, U. Delaware, Newark, DE, USA*
[7] *U. Graz, Graz, Austria*

ABSTRACT

We investigate the contribution of the radial component of the magnetic field in the solar wind interaction with Mars. We use Mars Global Surveyor Magnetometer and Electron Reflectometer data during the Science Phasing Orbits to gain a qualitative understanding of the magnitude of the radial magnetic field from the solar wind draping around the dayside of Mars. Using only data far away from the strong crustal magnetic sources, we find that the angle the magnetic field makes to the horizontal within the martian ionosphere has an average closer to zero than that outside the ionosphere. However, we find a much larger spread in angles inside the ionosphere. In addition, we find that the angle of inclination increases with increasing altitude and local time, but more spatial coverage is needed to quantify these relationships.

INTRODUCTION

Knowing the morphology of the magnetic field is very important to any study that involves the transport of ions and electrons along and across magnetic field lines. For example, ionospheric models compute the distribution of many plasma parameters as a function of altitude, considering chemistry and transport mechanisms in their calculations (*e.g.*, Choi *et al.*, 1998; Shinigawa and Cravens, 1989). When calculating vertical transport in a plasma, a strictly horizontal magnetic field inhibits much of the transport. However, even a small inclination in the magnetic field continued over a large horizontal distance allows substantial vertical plasma transport. Therefore, we analyze Mars Global Surveyor Magnetometer (MGS MAG) data to determine an average angle of inclination of magnetic field observed on the dayside of Mars. We compile statistics from MGS MAG data to determine how the draping acts as a function of position in the solar wind interaction with Mars.

The solar wind becomes "draped" around the martian dayside ionosphere as it approaches Mars because ionospheric currents cause the solar wind magnetic field to hang up in front of Mars. The result is that the magnetic field on the dayside of Mars is mostly locally horizontal, as shown in Figure 1. Inspecting the cartoon, we observe the following properties in the magnetic field direction. A small flare

takes magnetic field lines to higher altitude on the flanks than at local solar noon. In addition, with respect to the martian surface, the radial component of the magnetic field is expected to point away from Mars in the +y hemisphere and towards Mars in the -y hemisphere. Also, the absolute value of the angle should increase with increasing solar zenith angle.

SCIENCE PHASING ORBIT

The MGS Science Phasing Orbit (SPO) is a near polar orbit with a period of 11.6 hr. Its periapsis is at high northern latitude on the dayside of the planet, with solar zenith angles between 80°-90°. The local time of the orbit drifts from 10 a.m. to 6 p.m. during the period from March-August 1998. These orbits cover a great deal of altitude space, with periapsis at 175 km and apoapsis at 17,865 km. This is advantageous because the spacecraft traverses into the upstream solar wind on every orbit to observe solar wind conditions. Another advantage is that the periapsis altitude is low enough to be within the ionosphere, but high enough that the Electron Reflectometer (ER) may still be operated safely in SPO. Therefore, we are able to determine whether the spacecraft is within the ionosphere at any point along the orbit by looking for the appearance of oxygen Auger electrons at ~500 eV (Mitchell *et al.*, 2000). One disadvantage to the SPO data set is that the altitude and solar zenith angle vary simultaneously. In other words, one can not easily separate the effects of changing solar zenith angle from the effects of changing altitude because there is not a large range of solar zenith angle—altitude space covered, as shown in Figure 2. Similarly, the areographic latitudes are confined to mid-high northern latitudes. While some small northern crustal fields were identified (Acuña *et al.*, 1999), this data is spatially removed from the strong crustal fields of the southern highlands.

In contrast, the other MGS orbital geometries lack crucial features described above. The mapping orbit lacks the altitude coverage of SPO. Mapping is a near-circular orbit at ~400 km. The aerobraking orbits, while spanning a range in altitudes, go to such a low altitude that the ER is turned off for the periapsis pass. Therefore the electron data is not always available to determine whether the spacecraft is inside the ionosphere. Therefore, we restrict our analysis to the SPO data set at this point. The future addition of the remaining data will help the statistics where applicable.

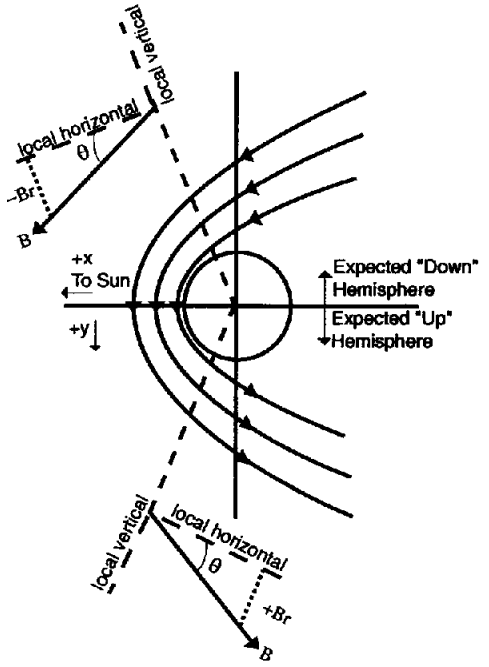

Fig. 1. This cartoon shows the magnetic field draping around Mars.

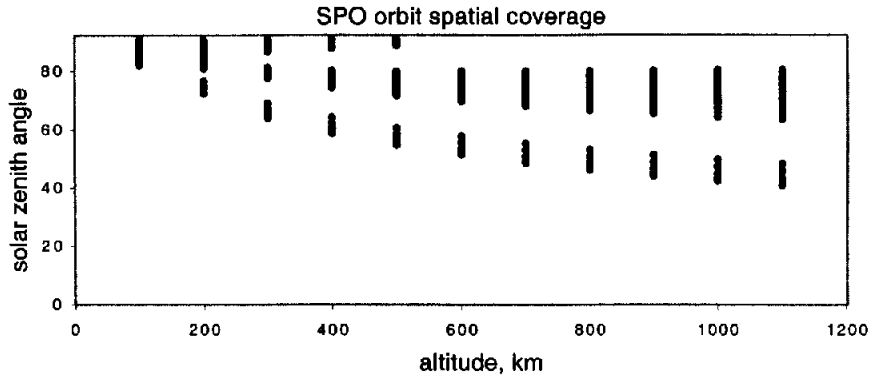

Fig. 2. The range of solar zenith angles covered by MGS is shown for each altitude bin. There is only data for all altitude bins at 80° solar zenith angle.

DATA ANALYSIS

We prepare the data for analysis by performing a series of rotations. First, we correct for the 3.5° aberration of the solar wind flow direction as seen by Mars. Next, we rotate the magnetic field into a coordinate system aligned with the upstream Interplanetary Magnetic Field (IMF) direction. This coordinate system is defined such that $B_{z\ IMF} = 0$, or the average IMF lies in ecliptic plane. However, the MGS spacecraft magnetic field often is too great to determine the direction of the IMF while in the pre-shocked solar wind. A rough estimate is given by rotating around the Mars-Sun line such that B_x changes sign in the magnetotail at y=0. As shown in Figure 1, the magnetic field direction changes from tailward to sunward in the induced magnetotail as one crosses from +y to –y. This transform is only possible if MGS crosses y=0 in IMF coordinates and assumes the solar wind is steady. Next, we locate ionospheric plasma using ER data. Finally, we calculate the magnetic field in the locally radial direction for each point on the orbit.

Next, we bin the data for statistics. We separate data by 100 km altitude bins for each orbit and include all data below 1200 km and less than 90° solar zenith angle. The result is 1320 bins from 110 orbits. We take the average radial magnetic field (B_r), magnitude ($|B|$), inclination angle (θ), and standard deviations thereof. We note the solar zenith angle, latitude, and local time of each bin. Based on that information, we determine the expected sign of the radial field for the bin. That is, if the bin is in the –y hemisphere, the expected sign is negative. Finally, we determine whether the spacecraft is inside or outside of the ionosphere for each bin.

At this point, we must make an important note about errors. This data is not yet calibrated to remove the spacecraft magnetic field of ~2 nT. The IMF $|B|$ at Mars is around 2-5 nT, on average. Therefore, the spacecraft field is a significant fraction of the IMF field. This prohibits us from determining the direction of the IMF accurately, leading us to look for the B_x sign change in the tail. Additionally, although the magnetic field in the sheath of Mars is typically 20-30 nT, we are focusing on a relatively small component of this field. The radial field is typically measured around 2-6 nT. Therefore, when looking at small angles of inclination, a spacecraft magnetic field contribution of a couple nT can constitute a large error. Until calibrations can be done, these results are only preliminary. Relative comparisons between parameters should be indicative of trends, but absolute numbers will change.

RESULTS

We investigate the inclination angle using all 1321 points. The average of the absolute value of the inclination angle is $|\ \theta_{dip}| = 0.20 \pm .15$ radians or $12° \pm 9°$. Next, we inspect the average using $-\theta_{dip}$ measured for the hemisphere with a down expected radial field and $+\theta_{dip}$ for the up expected hemisphere in the histogram in Figure 3. Using the negative of the measured angle in the "down" hemisphere maps

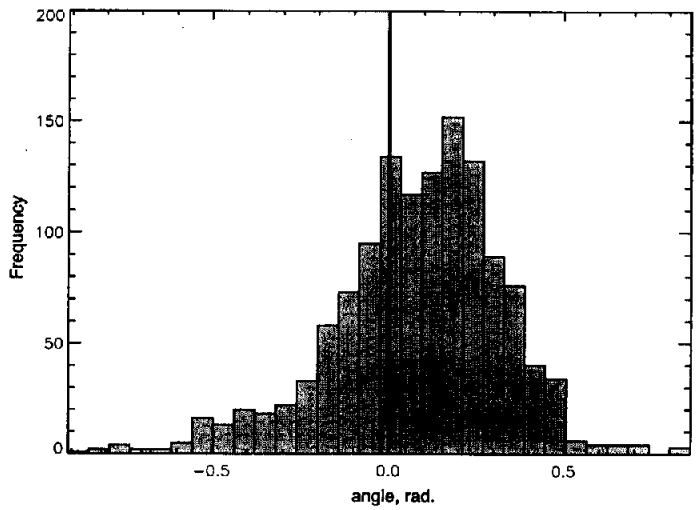

Fig. 3. This histogram shows the distribution of all inclination angles mapped to the +y hemisphere. That is, the negative of the angle is taken for those points in the –y hemisphere together with the positive of the angle for the points in the +y hemisphere.

all points to an expected positive inclination angle. Because the distributions for each hemisphere both have positive and negative values, this mapping process still yields some negative numbers. We find that $< \theta_{dip} >_{expect\ up\ all} = 0.09 \pm .24$ radians or $5° \pm 14°$.

Grouping by expected sign of the magnetic field, we plot the distributions separately for the up expected and down expected hemispheres in Figure 4. We find for the +y group, $<\theta_{dip}>_{up} = -0.06 \pm .2$ radians is the average angle using 338 points. Using 983 points, $<\theta_{dip}>_{down} = -0.14 \pm .2$ radians for the –y hemisphere. Note that the average angle obtained is down for the expected up group. That is probably due to the smaller sample size of the population. Approximately 3 times the number of points are expected to have negative B_r, giving that calculation better statistics. Therefore, we use only the expected down points for the following analysis.

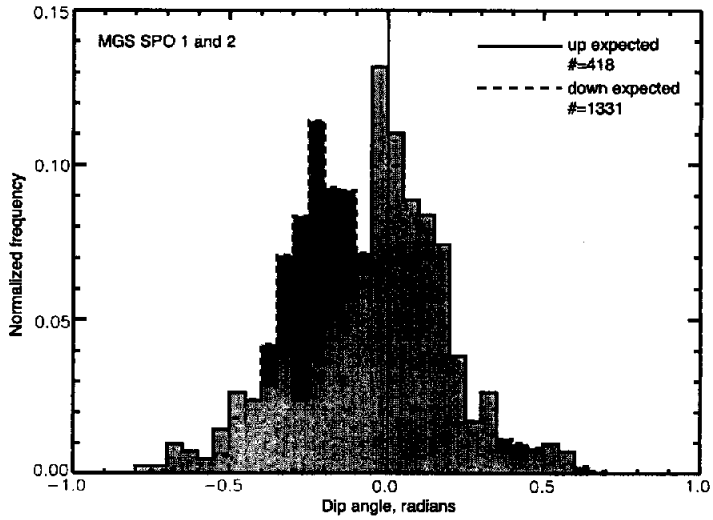

Fig. 4. The distributions for the down and up expected hemispheres are separated. The peak for "down" expected distribution is at lower than the "up" expected distribution.

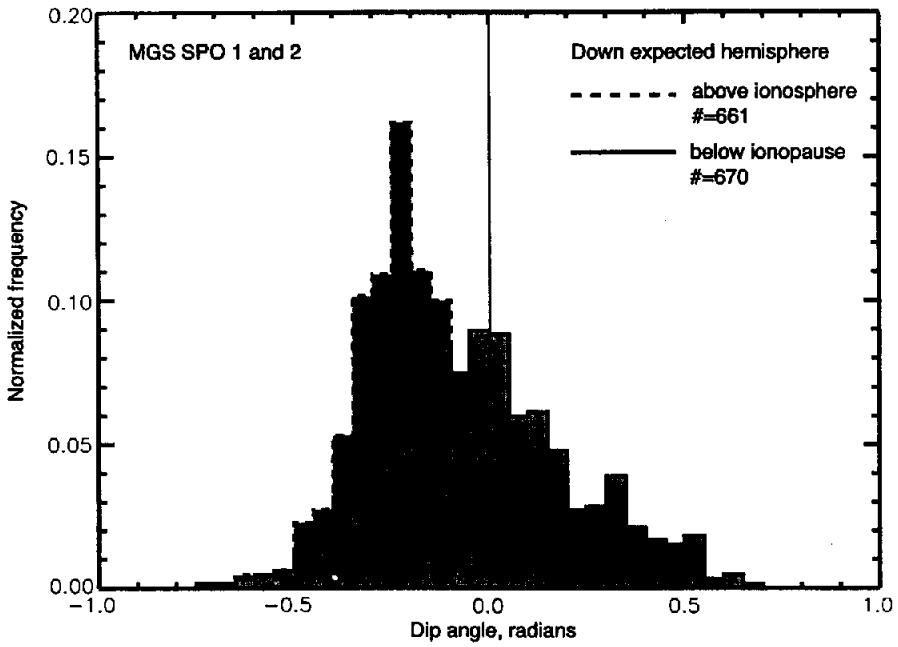

Fig. 5. Using only points from the down expected hemisphere, we plot the distributions grouped by whether the point was inside or outside of the ionosphere.

Next, we compare the radial field inside of the ionosphere compared to outside of the ionosphere in Figure 5. Data from above the ionosphere shows a much better defined draping geometry, with the average angle $\langle\theta_{dip}\rangle_{sheath} = 0.12 \pm .22$ radians or 7°. The distribution is much narrower than that from within the ionosphere. Data from within the ionosphere has larger spread in dip angle, but an average closer to zero. $\langle\theta_{dip}\rangle_{iono} = 0.04 \pm .26$ radians or 2° inside the ionosphere; however, very large positive and negative angles are observed. This is probably due to a selection effect in our data. The strong crustal magnetic fields at Mars have radial components in excess of 1500 nT (Acuña *et al.*, 1999) and locally elevate the altitude of the ionopause. Although we try to avoid these locations in the present analysis, some contribution remains. It is seen mostly in the "below ionopause" data because at any given altitude, one is more likely to be in the ionosphere when close to a crustal source than away from a crustal source. This selection effect causes the broad distribution and high values of dip angles within the ionosphere.

Besides the relationship with altitude due to the ionosphere, we look for variations in the inclination of the magnetic field with altitude. As shown in Figure 6, the dip angle increases with increasing altitude. A clear trend is observed in the line with square points, which uses the entire data set. A linear fit to the data using all solar zenith angles is shown in the gray dashed line. However, a solar zenith dependence is implicit by the orbital coverage, as displayed in Figure 2. We attempt to remove the solar zenith angle dependence by selecting only points from 75°-85° solar zenith angles. This is the only solar zenith angle range that includes all of the altitude bins. Doing so reduces the statistics. However, the increasing angle with increasing altitude trend continues, as shown in line marked with triangles in Figure 6.

Variations with local time and solar zenith angle were also checked. No strong correlations are seen with local time or solar zenith angle in this analysis. The dip angle increases with local time. However, the draping picture would have the dip angle go through zero at noon and be positive thereafter. That is not observed in this data set.

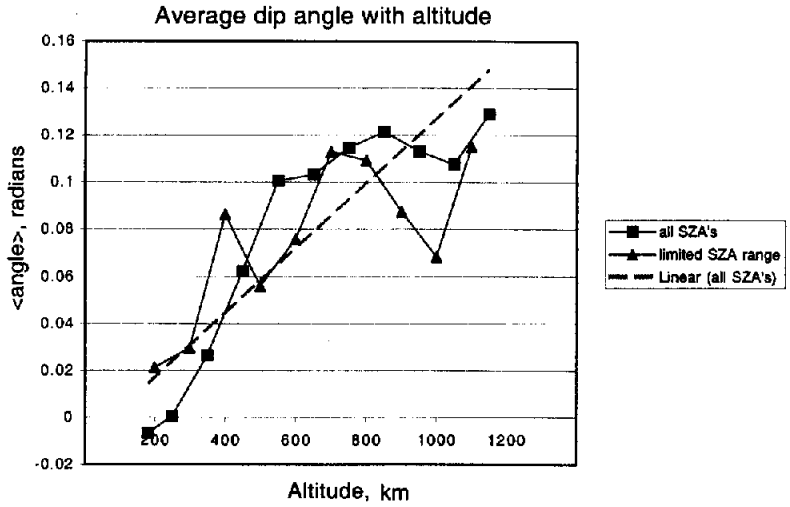

Fig. 6. We plot the inclination angle as a function of altitude using both (square) all points and (triangles) the points within 75°-85° solar zenith angle.

CONCLUSION

Once MGS MAG calibrations are complete, we will conduct a complete reanalysis of inclination angle measurements. But in the meantime, we find the following qualitative properties in the draping morphology of the magnetic field:

1) Draping is more well defined above the ionosphere than in the ionosphere.

2) The average inclination of the magnetic field is closer to zero inside the ionosphere than outside.

3) Crustal magnetic fields play a large role inside the martian ionosphere. This must be considered in plasma transport models.

4) Variations with altitude, solar zenith angle, and local time will have to await further analysis for conclusive relationships.

ACKNOWLEDGEMENT

This work was done while D.H.C. held an associateship from the National Research Council at NASA Goddard Space Flight Center.

REFERENCES

Acuña, M.H., J.E.P. Connerney, N.F. Ness, R.P. Lin, D.L. Mitchell, C.W. Carlson, J. McFadden, K.A. Anderson, H. Rème, C. Mazelle, D. Vignes, P. Wasilewski, and P. Cloutier. The History of Mars: Global Distribution of Crustal Magnetism Discovered by the Mars Global Surveyor MAG/ER Experiment, *Science*, **284**, 790, 1999.

Choi, Y.W., J. Kim, K.W. Min, A.F. Nagy, K.I. Oyama. Effect of Magnetic Field on the Energetics of Mars Ionosphere, *Geophys. Res. Lett.*, **25**, 2753, 1998.

Mitchell, D.L., R.P. Lin, H. Rème, D.H. Crider, P.A. Cloutier, J.E.P. Connerney, M.H. Acuña, and N.F. Ness. Oxygen Auger Electrons Observed in Mars' Ionosphere, *Geophys. Res. Lett.*, **27**, 1871, 2000.

Shinagawa, H. and T.E. Cravens. A One Dimensional Multispecies Magnetohydrodynamic Model of the Dayside Ionosphere of Mars, *J. Geophys. Res.*, **94**, 6506, 1989.